WARWICK
THE UNIVERSITY OF WARWICK

Permanent WRAP URL:
http://wrap.warwick.ac.uk/96724

warwick.ac.uk/lib-publications

Tracking a hysteretic and disorder-broadened phase transition via the electromagnon response in improper ferroelectrics

C. D. W. Mosley[1], D. Prabhakaran[2] and J. Lloyd-Hughes[1]

[1]Department of Physics, University of Warwick, Gibbet Hill Road, Coventry CV4 7AL, UK

[2]Department of Physics, Clarendon Laboratory, University of Oxford, Parks Road, Oxford OX1 3PU, UK

Abstract. We demonstrate that electromagnons can be used to directly probe the nature of a phase transition between magnetically ordered phases in an improper ferroelectric. The antiferromagnetic/paraelectric to antiferromagnetic/ferroelectric phase transition in $Cu_{1-x}Zn_xO$ ($x = 0, 0.05$) alloys was tracked via the electromagnon response using terahertz time-domain spectroscopy, on heating and cooling through the phase transition. The transition was found to exhibit thermal hysteresis, confirming its first-order nature, and to broaden under the influence of spin-disorder upon Zn substitution. The energy of the electromagnon increases upon alloying, as a result of the non-magnetic ions modifying the magnetic interactions that give rise to the multiferroic phase and electromagnons. We describe our findings in the context of recent theoretical work that examined improper ferroelectricity and electromagnons in CuO from phenomenological and first-principles approaches.

Introduction

Multiferroic materials have increasingly inspired interest in recent years due to their potential technological applications; specifically magnetoelectric coupling, where the magnetic order can be influenced by an applied electric field and vice versa, may have intriguing applications in spintronics [1, 2, 3] and novel electronic components [4, 5]. Of particular interest are improper ferroelectric multiferroics, in which ferroelectricity is induced by frustrated magnetic interactions, forming a magnetic state that breaks inversion symmetry, for instance an incommensurate spin-cycloid [6, 7]. Strong magnetoelectric coupling can occur in such materials [8, 9], however the improper ferroelectric phase generally occurs only at low temperatures, typically below $\sim 70\,\mathrm{K}$ [8]. For many of the technological applications to be realized, room-temperature magnetoelectrics are strongly desired.

The static polarization in an improper ferroelectric phase can be understood as arising from the spin current or inverse Dzyaloshinskii-Moriya (DM) interaction [6], which induces a polarization $\mathbf{P} \propto (\mathbf{S}_n \times \mathbf{S}_{n+1})$, where $\mathbf{S}_n$, $\mathbf{S}_{n+1}$ are adjacent spins in the cycloid. The induced static polarization in many improper ferroelectric materials is weak (typically $< 1\,\mu\mathrm{C\,cm^{-2}}$) [8]. Further, improper ferroelectrics exhibit dynamic magnetoelectric coupling, whereby an oscillating electric field couples to a spin wave, or magnon. This results in a novel quasiparticle excitation at terahertz frequencies - the electromagnon [10, 11, 12, 13, 14, 15]. Two distinct mechanisms that give rise to electromagnons have been discussed in the literature: Dzyaloshinskii-Moriya electromagnons, which are eigenmodes of a spin-cycloid induced by the DM interaction [13] and couple directly to oscillating electric fields [16]; and exchange-striction electromagnons, which arise from a modulation of the isotropic Heisenberg exchange interaction proportional to a $(\mathbf{S}_i \cdot \mathbf{S}_j)$ term in the Hamiltonian [17, 18]. Electromagnons have been observed at low temperatures ($< 70\,\mathrm{K}$) in materials such as $R\mathrm{MnO_3}$ and $R\mathrm{Mn_2O_5}$ (R = rare earths) [10, 11, 12, 13, 14], and at high temperatures in $\mathrm{Cu_{1-x}Zn_xO}$ alloys ($213\,\text{-}\,230\,\mathrm{K}$ in $x = 0$ and $159\,\text{-}\,190\,\mathrm{K}$ in $x = 0.05$) [15, 19]. An IR and Raman-active electromagnon has also recently been observed at up to 250K in a z-type hexaferrite [20].

In this paper we first review the salient features of improper ferroelectricity in pure and spin-disordered CuO. We then demonstrate that the electromagnon can be used to probe order-to-order phase transitions, such as found in CuO, where one phase is an improper ferroelectric. A detailed study of the antiferromagnetic/paraelectric to antiferromagnetic/ferroelectric phase transition using terahertz time-domain spectroscopy highlighted the hysteretic nature of the phase transition, and the influence of spin-disorder.

Improper ferroelectricity in CuO

A promising material system in the study of improper ferroelectrics is cupric oxide (CuO), which exhibits a magnetically-induced ferroelectric phase with spin-cycloidal ordering at $\sim 230\,\mathrm{K}$ [21]. CuO has a monoclinic crystal structure with space group $C2/c$, which can be visualized as zig-zagging Cu-O-Cu chains along the [101] and [10$\bar{1}$] directions. The magnetic phases of CuO have previously been characterized by neutron diffraction [22, 23] and ultrasound velocity measurements [24]. Below $213\,\mathrm{K}$, the dominant magnetic interaction is antiferromagnetic superexchange between spins in $\mathrm{Cu^{2+}}$ chains in the [10$\bar{1}$] direction ($J_{\mathrm{AFM}} \sim 80\,\mathrm{meV}$) [25]. Weaker ferromagnetic superexchange interactions occur between spins in adjacent spin chains along the [101] ($J_{\mathrm{FM1}} \sim 5\,\mathrm{meV}$) and [010] ($J_{\mathrm{FM2}} \sim 3\,\mathrm{meV}$) directions [25]. As the ratio of interchain to intrachain interactions is about 0.1, CuO can be described as a quasi-1D collinear Heisenberg antiferromagnet in the low temperature (AF1) phase [26, 27], consisting of two interpenetrating $\mathrm{Cu^{2+}}$ sublattices with spins aligned along the b-axis. At $213\,\mathrm{K}$ the spins on one sublattice flop into the ac-plane [28] and form an incommensurate spin-cycloid phase (AF2) with magnetic ordering vector $\mathbf{q} = (0.506, 0, -0.483)$ [22, 23]. A magnetically-induced ferroelectric polarization in this phase occurs in the b-direction [21], which also exhibits ferroelectric hysteresis loops [21]. An electromagnon occurs in the multiferroic AF2 phase, which is active for oscillating electric fields parallel to the [101] direction and its strength is linked to the size of the static polarization [15]. Between $229.3\,\text{-}\,230\,\mathrm{K}$ an intermediate commensurate, collinear magnetic phase (AF3) forms [24], and above $230\,\mathrm{K}$ is the paramagnetic phase (PM). The first-order nature of the AF1\,-\,AF2 phase transition has been observed by specific heat [29, 30, 31] measurements.

The occurrence of the AF1\,-\,AF2 phase transition can be understood using the mechanism proposed by Yablonskii [28], where a biquadratic exchange term stabilizes the low temperature AF1 state. The free energy of a system is given by $F = E - TS$, where T is temperature and S is entropy. The energy of the interactions between the spin chains in the [10$\bar{1}$] direction is given by Yablonskii as [28]:

$$E = \sum_n \big[J_1 \mathbf{S}_n \cdot \mathbf{S}_{n+1} + J_2 \mathbf{S}_n \cdot \mathbf{S}_{n+2} + I(\mathbf{S}_n \cdot \mathbf{S}_{n+1})(\mathbf{S}_n \cdot \mathbf{S}_{n+2}) \big], \tag{1}$$

where J_1 is the nearest-neighbour ferromagnetic exchange interaction, J_2 is the next-nearest-neighbour

antiferromagnetic exchange interaction, and I is the biquadratic exchange interaction. Taking a mean-field approximation with the spatially averaged value of the spins as S_{av}, the AF1 state will have a lower energy for $S_{av}^2 > J_1^2/8IJ_2$. As temperature increases, the value of S_{av} decreases, therefore at some point the AF2 state has a lower energy and the system undergoes a phase transition. The value of S_{av} is effectively controlled by disorder, which can be influenced in a number of ways, the simplest being a change in temperature changing the form of F and driving the phase transition. Analogously a change in the entropy of the system will also change the form of F; evidence for this has been provided by optical-pump X-ray probe measurements on CuO [32]. With the system held just below the phase transition at $207\,$K, electrons were excited above the charge-transfer bandgap by $800\,$nm femtosecond pulses, introducing spin-disorder into the system and thus changing the entropy. A larger reduction in the intensity of the X-ray peak associated with the AF1 phase compared to the peak associated with the AF2 phase was observed, hinting at an ultrafast phase transition driven by the introduction of spin-disorder.

Quenched spin-disorder in CuO

An alternative method of introducing spin-disorder into the system which may be more desirable for technological applications is by alloying with non-magnetic ions: theoretical investigations predict that the introduction of non-magnetic impurities may stabilize the multiferroic phase at higher temperatures than the pure case [33], and that hydrostatic pressure can broaden the multiferroic phase above room temperature [34]. Alloying of $Cu_{1-x}M_xO$ with a non-magnetic ion M has been demonstrated to broaden the multiferroic phase, for $M = $ Zn, Co by studying the static ferroelectric polarization along b [35], and for $M = $ Zn using the electromagnon response [19]. Spin-disorder introduced by the non-magnetic ions breaks up long-range correlations between spins and suppresses the Néel temperatures [36], reducing the AF1 - AF2 transition to $\sim 159\,$K and the AF2 - paraelectric transition to $\sim 190\,$K for $M = $ Zn and $x = 0.05$ [19]. This equates to broadening the multiferroic phase from $17\,$K to $30\,$K. The electromagnon is preserved in the AF2 phase of $Cu_{0.95}Zn_{0.05}O$, with the same E $\|$ [101] selection rule as in the pure case [15, 19].

The change in magnetic or lattice structure at a first-order phase transition is associated with many functional properties that emerge in the ordered phases [37, 38]. First-order phase transitions are characterized by a latent heat, due to a difference in entropy between the two phases requiring the system to absorb a fixed amount of energy in order for the transition to occur. This leads to phase coexistence, where some parts of the material have undergone the transition and others have not. In alloys, the dopant concentration can influence the nature of both the phase transition and the functional properties of interest [37, 38]. Imry and Wortis demonstrated that a first-order phase transition can be broadened by the introduction of quenched random disorder into the system [39]. The correlation length of interactions can be reduced by local impurities, causing different parts of the material to undergo a first-order phase transition at different temperatures, appearing to round off the discontinuity in the order parameter or other related experimental observables.

Experimentally, a phase transition can be classified as first-order by the observation of a discontinuous change in the order parameter and a latent heat, phase coexistence, or hysteresis with respect to a control variable (such as temperature or external magnetic field). It is not necessary to observe hysteresis in the order parameter, as many experimental observables can be hysteretic over a first-order phase transition, exemplified by the observation of hysteresis in magneto-optical properties during the melting of a superconducting vortex-solid [40]. Broadening of first-order phase transitions by disorder may obscure discontinuities in experimental observables, making the latent heat of the transition difficult to determine [38, 39]. As such, hysteresis or phase coexistence are required to observe the first-order nature of the transition.

Ideally, one should look for hysteresis in an experimental observable that is uniquely linked to the multiferroic state (e.g. the ferroelectric polarization), rather then observables that only change marginally across the transition (e.g. ultrasound velocity, magnetization). The pyroelectric current method is commonly used to study the polarization of magnetically-induced ferroelectrics: a large electric field is applied while in the multiferroic state, which is then removed and the pyroelectric current on cooling or heating through the ferroelectric/paraelectric phase transition is recorded and integrated to yield the polarization. This method often only measures the polarization as the temperature is swept out of the multiferroic state, and it is therefore challenging to study thermal hysteresis.

As the electromagnon in $Cu_{1-x}Zn_xO$ is experimentally observed via the dynamic excitation of the ferroelectric polarization, it cannot be observed without the AF2 phase being present within the material. The excitation energy and absorption strength of the electromagnon in CuO have previously been shown to closely track the size of the static polarization $P_{[010]}$ in the AF2 phase [15], which is in turn intimately linked to the magnetic order. Theoretical investiga-

tions of electromagnons in CuO indicate that the electromagnon energy is related to the size of the magnetoelectric coupling parameters in the spin Hamiltonian [41]. Hence the properties of the electromagnon can provide a direct probe of the magnetic interactions giving rise to multiferroicity, and their evolution as the material undergoes a phase transition.

Experimental Methods

Single crystals of CuO and $Cu_{0.95}Zn_{0.05}O$ were prepared by methods described elsewhere [42, 19]. Samples of both materials were cut from the boule and aligned using Laue X-ray diffraction to have a $(10\bar{1})$ surface normal, giving the [101] and [010] crystallographic directions in the plane. Samples were double-side polished, resulting in a thickness of 1.28 mm for the CuO and 0.89 mm for the $Cu_{0.95}Zn_{0.05}O$.

The electromagnon response of the samples was measured by terahertz time-domain spectroscopy (THz-TDS) [43, 44]. THz-TDS directly measures both the amplitude and the phase of the THz electric field after transmission through the sample, allowing the complex refractive index of the sample $\tilde{n} = n + i\kappa$ to be determined. In order to avoid the influence of absorption from the broad A_u^3 phonon mode [19] or birefringent effects resulting from sample misalignment [15, 45], the relative change in terahertz absorption coefficient with respect to the low temperature AF1 phase $\Delta\alpha = \alpha(T) - \alpha(T_{AF1})$, where $\alpha = 2\omega\kappa/c$, was used instead of a vacuum reference.

Single-cycle, linearly-polarized pulses of THz radiation were generated using a wide-area interdigitated GaAs photoconductive emitter and detected via electro-optic sampling in ZnTe. The entire THz path inside the spectrometer was purged with dry N_2 gas in order to remove the influence of water vapour, which has strong absorption features at THz frequencies [46]. Samples were mounted in a cryostat such that the THz electric field was parallel to the [101] crystallographic direction, where the electromagnon absorption is strongest [15, 45], and positioned at the sample focus of the spectrometer. On heating and cooling the sample temperature was increased or decreased in discrete steps of 0.1 K, with a wait time of 2 minutes before beginning data acquisition at each step, to ensure the sample was in thermal equilibrium with the cold finger of the cryostat. Data acquisition took 5 minutes at each step. The wait time and measurement time was the same for all scans on both samples.

Results and Discussion

Electromagnon response over the AF1 - AF2 phase transition

To investigate the effects of zinc alloying on the AF1 - AF2 phase transition in $Cu_{1-x}Zn_xO$, the change in terahertz absorption coefficient $\Delta\alpha$ over the AF1 - AF2 phase transition is presented in Fig. 1(a) for $x = 0$ and Fig. 1(b) for $x = 0.05$. Samples were heated over a 5 K range around the AF1 - AF2 transition temperatures ($\sim$ 213 K for $x = 0$ and $\sim$ 160 K for $x = 0.05$), and $\Delta\alpha$ measured at each step. The electromagnon is observable in both samples as a peak in $\Delta\alpha$, at 0.72 THz for $x = 0$ and at 0.85 THz for $x = 0.05$, consistent with previous observations [15, 19]. In the case of pure CuO, the electromagnon onset is rapid, with $\Delta\alpha$ rising from zero to a maximum in around 1.5 K. Comparatively in the Zn-alloyed sample the onset is much slower, with the rise in absorption occurring in around 3.5 K. At higher frequencies, a broad shoulder to the electromagnon around 1.2 THz is also visible in the $x = 0$ sample, and has a similar temperature-dependent onset as the main electromagnon. Intriguingly, this higher-frequency shoulder is not observed in the $x = 0.05$ sample, suggesting that this mode may be either shifted in energy, suppressed or even disrupted entirely upon alloying with zinc.

The electromagnon strength is intimately linked to the incommensurate magnetic order in the multiferroic phase, and therefore can give insight into the nature of the magnetic ordering. To evaluate the properties of the observed electromagnons in the $Cu_{1-x}Zn_xO$ alloys, and to allow comparison with each other and others reported in the literature, a Drude-Lorentz oscillator model was used to fit the data. This gives the temperature-dependent change in dielectric function $\Delta\epsilon(\omega) = \epsilon(\omega, T_2) - \epsilon(\omega, T_1)$ as

$$\Delta\epsilon(\omega) = \frac{\Delta\epsilon \cdot \omega_0^2}{\omega_0^2 - \omega^2 - i\omega\Gamma}, \tag{2}$$

where $\Delta\epsilon$ is the oscillator strength, ω_0 is the oscillator frequency and Γ is the linewidth. Fits to the experimentally measured change in dielectric function $\Delta\epsilon(\omega)$ of $Cu_{1-x}Zn_xO$ with respect to the low-temperature phase are presented in Fig. 2(a) for $x = 0$ at 213 K, and in Fig. 2(b) for $x = 0.05$ at 161 K. A combination of two oscillators was required when fitting $\Delta\epsilon(\omega)$ for $x = 0$, with the main electromagnon (blue) having a strength $\Delta\epsilon = 0.065$, frequency $f = 0.71$ THz and linewidth $\Gamma = 2.0$ THz, while the broader shoulder mode (green) has $\Delta\epsilon = 0.025$ and linewidth $\Gamma = 8.0$ THz. In order to correctly model the high-frequency features, the frequency of the shoulder mode was fixed at 1.2 THz. Comparatively $\Delta\epsilon(\omega)$ for $x =$
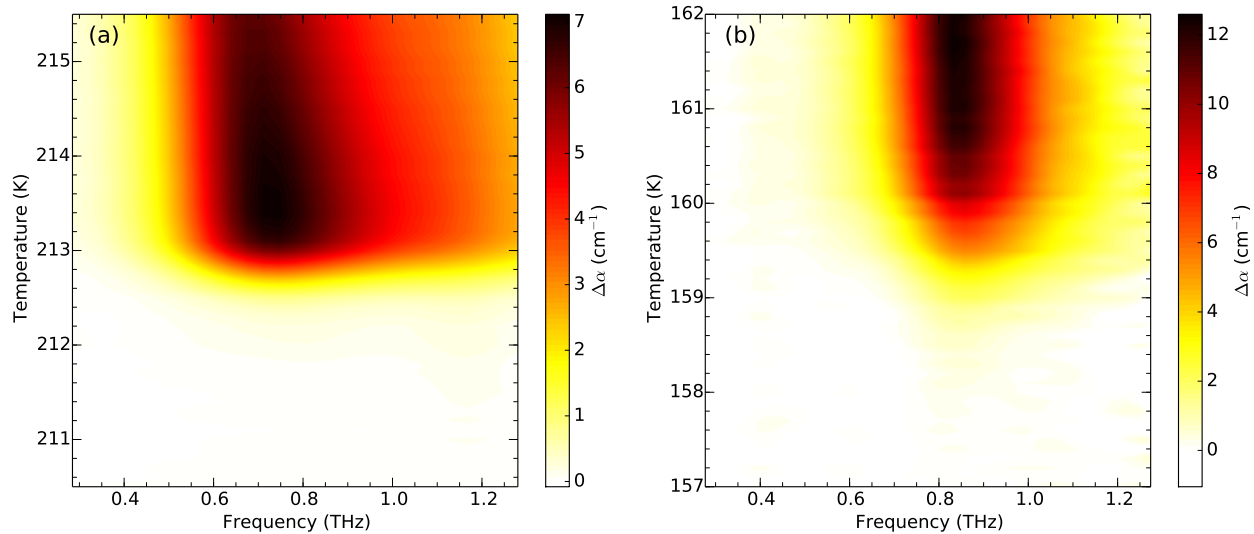
Figure 1. Change in terahertz absorption coefficient $\Delta\alpha$ with respect to the low temperature phase over the AF1 - AF2 phase transition in $Cu_{1-x}Zn_xO$ alloys, with **(a)** $x = 0$ and **(b)** $x = 0.05$.

0.05 was well fit by a single oscillator (red), with strength $\Delta\epsilon = 0.072$, frequency $f = 0.84\,THz$ and linewidth $\Gamma = 2.0\,THz$. All values are consistent with those reported previously in the literature [15, 19]. Experimental bandwidth was limited to $1.3\,THz$ in $x = 0.05$ due to the softening and broadening of the phonon modes upon alloying with zinc [19].

To quantify the evolution of the electromagnon across the phase transition in both samples, similar Drude-Lorentz fits to those in Fig. 2(a) and 2(b) were performed at each temperature step on cooling the samples over the AF1 - AF2 phase transition. Fit parameters of oscillator strength, oscillator frequency and linewidth for $x = 0$ are presented in Figs. 2(c) - 2(e). The strength of both oscillators begins increasing sharply at $212.2\,K$, reaching a maximum in around $1.2\,K$. The frequency of the main electromagnon mode continually red-shifts with increasing temperature over the phase transition, decreasing from $0.73\,THz$ at $212.2\,K$ to $0.69\,THz$ at $214.2\,K$. The linewidth of both oscillators remains constant over the majority of the phase transition, decreasing slightly in width from when the excitation first begins to emerge. Fit parameters for $x = 0.05$ are presented in Figs. 2(f) - 2(h). The strength of the oscillator shows a gentler, broader increase with temperature, starting to increase around $157.8\,K$ and reaching a maximum after around $3.5\,K$. Both frequency and linewidth demonstrate the same trends seen for $x = 0$, with the frequency red-shifting from $0.9\,THz$ at $167\,K$ to $0.85\,THz$ at $161\,K$, and the linewidth remaining constant except for initially when the oscillator strength was very small. Values of frequency and linewidth are presented for temperatures at which the oscillator strength was large enough to provide a meaningful fit.

Theoretical investigations of electromagnons in CuO [41] have modeled the magnetic properties using a spin Hamiltonian of the form

$$\widehat{H} = \sum_{ij} J_{ij}\mathbf{S}_i \cdot \mathbf{S}_j + \mathbf{D}_{ij} \cdot (\mathbf{S}_i \times \mathbf{S}_j)$$
$$- \sum_i (\mathbf{K} \cdot \mathbf{S}_i)^2 + \widehat{H}_{\mathrm{me}}, \qquad (3)$$

where the first term accounts for superexchange interactions between adjacent spins $\mathbf{S}_i$, the second term decribes the DM interaction, the third term describes single-ion anisotropy, and the final term accounts for magnetoelectric coupling. Increases to the magnitude of $\mathbf{D}$ and $\mathbf{K}$, the DM and anisotropic coupling constants respectively, were found to enhance the electromagnon energy, directly linking the electromagnon energy to the strength of the interactions responsible for the AF2 phase. An electromagnon frequency of $0.73\,THz$ (energy $\sim 3\,meV$) as observed at $212.3\,K$ in Fig. 2(d) corresponds to $|\mathbf{D}| = 0.4\,meV$ and $|\mathbf{K}| = 0.6\,meV$ [41]. The frequency of the electromagnon mode in $Cu_{1-x}Zn_xO$ is observed to increase considerably upon alloying of $x = 0.05$, suggesting that zinc alloying alters the interactions between spins. From reference [41], an increase in electromagnon frequency to $0.9\,THz$ (energy $\sim 3.7\,meV$) as observed at $158.1\,K$ in Fig. 2(g) corresponds to either an increase in $|\mathbf{D}|$ to $0.65\,meV$, or an increase in $|\mathbf{K}|$ to $0.95\,meV$, or a smaller simultaneous increase in both.
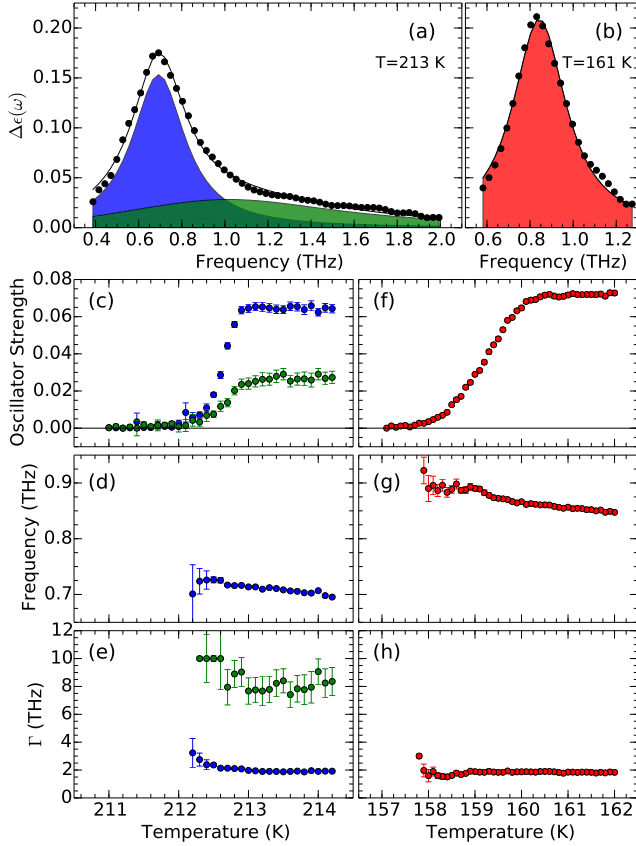
Figure 2. **(a)** and **(b)** are the temperature-induced change in dielectric function $\Delta\epsilon(\omega)$ (black dots) across the AF1-AF2 phase transition in $Cu_{1-x}Zn_xO$ alloys with $x = 0$ and $x = 0.05$, respectively. Black lines are Drude-Lorentz fits comprised of a single oscillator (red shaded area) for $x = 0.05$ and two oscillators (blue and green shaded areas) for $x = 0$. **(c)**, **(d)** and **(e)** are the best fit parameters of the oscillator strength, frequency and linewidth Γ, respectively, over the phase transition for $x = 0$. **(f)**, **(g)** and **(h)** are the corresponding best fit parameters over the phase transition for $x = 0.05$. The color of the data points corresponds to the oscillator they refer to in **(a)** and **(b)**.

This alteration of magnetic interactions may be understood with reference to the "order-by-disorder" mechanism proposed by Henley [47], which describes the stabilization of a non-collinear spin state with respect to a collinear spin state, as quenched disorder favors spins in different sublattices to be oriented perpendicular to each other. Simulations have shown that the multiferroic phase in CuO can be stabilized by alloying with non-magnetic ions [35]. Density functional theory (DFT) calculations for pure CuO give a difference in energy between the AF2 and AF1 phase $\Delta E = E_{AF2} - E_{AF1} = 2.15\,\mathrm{meV}$ per Cu, parameterised by $\Delta E = 4IS^4$ where $S = 1/2$ and I is the biquadratic exchange coupling constant. Similar DFT calculations for alloyed CuO show a reduction
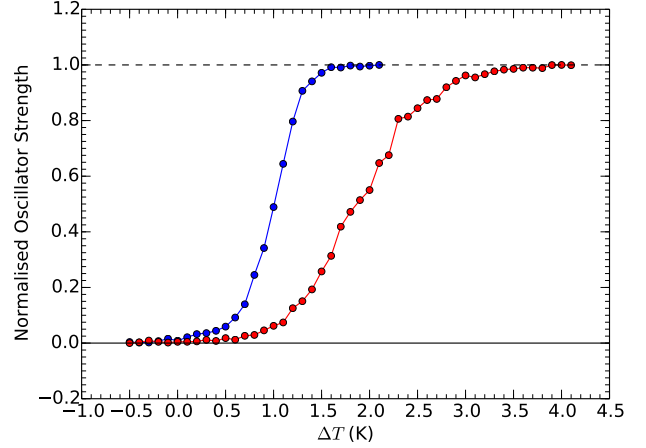

Figure 3. Temperature dependent change in the oscillator strength of the electromagnon, over the AF1-AF2 phase transition, in $Cu_{1-x}Zn_xO$ alloys with $x = 0$ (blue points) and $x = 0.05$ (red points).

in the energy difference between the AF1 and AF2 states, estimating a reduction to $\Delta E = 1.94\,\mathrm{meV}$ per Cu for 5% zinc alloying. Two contributions to this reduction in energy were determined, with similar sized contributions for Zn alloying: modification of the biquadratic exchange interactions between the non-magnetic impurity and spins on the other sublattice, and an alteration of the local Weiss field around the non-magnetic impurities which acts to orient spins on the same sublattice perpendicular to those on the other sublattice by the Henley mechanism. This change in the Weiss field around the non-magnetic ions will alter the value of the anisotropic coupling constant **K**. A change in the DM coupling constant **D** can also occur as the DM interaction is sensitive to the Cu-O-Cu bond angle [6], which changes on alloying with zinc [15].

Disorder-broadening of the AF1-AF2 phase transition

For a direct comparison of the width of the AF1-AF2 phase transition for $x = 0$ and $x = 0.05$, Fig. 3 presents the oscillator strength of the two main modes from Figs. 1(a) and 1(b), normalized by their maximum value. The change in temperature ΔT is defined relative to the temperature at which the derivative of the oscillator strength with respect to temperature, $d(\Delta\epsilon)/dT$, increases from zero. The oscillator strength rises from zero to maximum in around $\Delta T_1 = 1.6\,\mathrm{K}$ for $x = 0$ and $\Delta T_2 = 3.9\,\mathrm{K}$ for $x = 0.05$. Thus a broadening of $2.3\,\mathrm{K}$ occurs for the AF1-AF2 phase transition upon alloying with 5% zinc, a ratio of $\Delta T_2/\Delta T_1 = 2.6$.

This broadening of the phase transition occurs due to the quenched random spin-disorder introduced upon

alloying with non-magnetic zinc ions. As mentioned previously, CuO can be regarded as a quasi-1D colinear Heisenberg antiferromagnet in the commensurate AF1 phase, consisting of spin chains along the $[10\bar{1}]$ direction. Alloying of $x = 0.05$ has been shown to suppress the Néel temperatures in $Cu_{1-x}Zn_xO$ [19] due to spin disorder breaking communication along the spin chains, which reduces the correlation length to the average impurity separation. During formation of the alloy, the local impurity density in the melt will vary slightly around an average value, and this variation becomes frozen-in as the alloy crystallizes. The correlation length of interactions therefore varies depending on the local impurity density, and hence so does the local Néel temperature. In local regions where the impurity density is higher than average the Néel temperature will be lower than average, and vice versa. This causes the AF1-AF2 phase transition to occur over a range of temperatures depending on the local impurity density [39].

The electromagnon excitation cannot be observed without the presence of the AF2 phase, as its strength is strongly linked to the size of the magnetically-induced static polarization in the AF2 phase [15]; as such the normalised oscillator strength in Fig. 3 can be interpreted as the ratio of the amount of AF2 to AF1 phase present in the sample. The emergence of the electromagnon upon heating the sample through the phase transition therefore corresponds to initial nucleation of the AF2 phase. The local variation in Néel temperature resulting from quenched spin-disorder in the $x = 0.05$ sample causes nucleation to occur at different temperatures in different regions of the sample, evidenced by the broader increase in electromagnon strength with temperature.

Hysteresis in the electromagnon response

Temperature-dependent hysteresis is one of the experimental signatures of a first-order phase transition, and should be present in many experimental observables related to an order parameter involved in the phase transition. As a natural extention to the analysis of Fig. 3, we show here that the strength of the electromagnon can be used to observe hysteretic behaviour at the AF1-AF2 phase transition on heating and cooling of the sample.

The electromagnon response in $Cu_{1-x}Zn_xO$ alloys as the temperature is first increased and then decreased across the AF1-AF2 phase transition is presented in Fig. 4(a) for $x = 0$ and in Fig. 4(b) for $x = 0.05$. Hysteresis is clearly visible in both pure and zinc alloyed samples, with the centre of the phase transition occurring at higher temperatures when temperature was increased over the phase transition compared to when it was decreased. The centre points of the
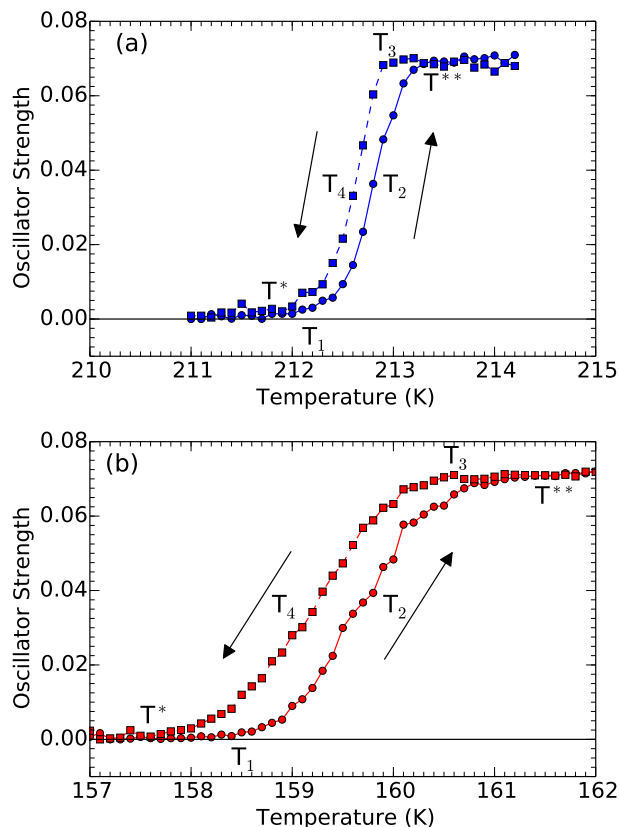

Figure 4. Temperature-dependent hysteresis observed in the electromagnon response across the AF1-AF2 phase transition in $Cu_{1-x}Zn_xO$ alloys with **(a)** $x = 0$ and **(b)** $x = 0.05$. Upwards facing arrows denote increasing temperature (also denoted by solid circles) and downwards facing arrows denote decreasing temperature (solid squares). T_1 and T_3 are the temperatures at which the oscillator strength begins to deviate significantly from zero or the maximum, respectively. T_2 and T_4 are the mid-points of the phase transition during heating and cooling, respectively. T^{**} and T^* are the limits of metastability for superheating and supercooling, respectively.

increasing and decreasing temperature measurements, T_2 and T_4 respectively, are separated by $0.2\,\mathrm{K}$ in the $x = 0$ sample and $0.5\,\mathrm{K}$ in the $x = 0.05$ sample. The ratio between these values of 2.5 is similar to the degree of disorder-induced broadening of the phase transition observed in Fig. 3. Subsequent heating and cooling measurements reproduced the same hysteretic behaviour.

Here we consider a simple phenomenological description of the free energy with reference to Landau theory for a first-order phase transition, in order to describe the observed hysteretic behaviour. Advanced treatments more suitable for multiferroics have been reported, for instance including the magnetoelectric coupling between a uniform polarization and incommensu-
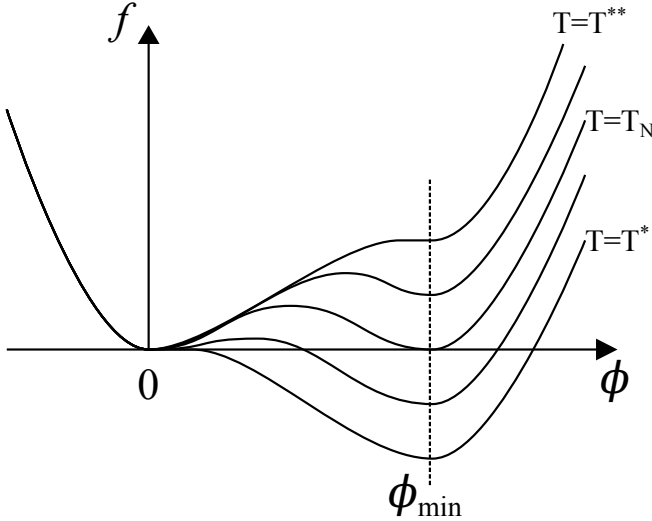
Figure 5. Schematic diagram of the free energy f as temperature is increased and decreased across a first-order phase transition, with respect to the order parameter ϕ. T_N is the thermodynamic transition temperature, T^* is the metastable limit of supercooling, and T^{**} is the metastable limit of superheating.

rate magnetic order [48], or non-local Landau theories that describe spin-lattice coupling [49, 24]. The free energy density of the system with respect to a control variable, here taken to be the temperature T, can be expressed in terms of the order parameter ϕ. One possibility by which a first-order phase transition can occur is if the free energy density has a third-order term in ϕ, such as

$$f(T,\phi) = \frac{r(T)}{2}\phi^2 - w\phi^3 + u\phi^4, \qquad (4)$$

where w and u are positive and temperature-independent. In many systems third-order terms in ϕ are forbidden by symmetry. In such a case, a first-order phase transition can still occur if the free energy has a negative quartic term with a positive sixth-order term for stability, such as

$$f(T,\phi) = \frac{r(T)}{2}\phi^2 - w\phi^4 + u\phi^6. \qquad (5)$$

Fourth- and sixth-order terms can arise in magneto-electrics, for instance as a result of strong spin-lattice coupling [49], and such Landau models have been developed for CuO [24, 50]. Substantial spin-lattice coupling has been reported in $Cu_{1-x}Zn_xO$ as the phonon modes alter across the AF1-AF2 transition [19]. Note that the order parameter can be complex, to allow for non-collinear magnetic states [50].

A schematic diagram of the form of the free energy density around a first-order phase transition with respect to ϕ is presented in Fig. 5. Here we assume the order parameter for CuO to be represented by the magnetisation along b for one magnetic sublattice, which is zero in the spin-cycloid phase (AF2) and a finite value ϕ_{min} in the antiferromagnetic AF1 phase. When the temperature is higher than the thermodynamic transition temperature T_N the free energy has one global minimum, at $\phi = 0$, corresponding to the AF2 phase. At $T = T_N$ there are two minima to the free energy and the AF1 and AF2 phases can coexist. These minima are located at $\phi = 0$ and $\phi = \phi_{min}$ and separated by an energy barrier. When the temperature drops below T_N the global minimum of the system shifts to ϕ_{min}, corresponding to the AF1 phase; however $\phi = 0$ remains a local minimum of the system, with the two phases still separated by an energy barrier, which will reduce in height with decreasing temperature. Eventually the height of the energy barrier will reduce to zero at the limit of metastability for supercooling $T = T^*$, the temperature at which $d^2f/d\phi^2 = 0$ at $\phi = 0$ and none of the AF2 phase can exist. An analogous process occurs for increasing temperature, where ϕ_{min} continues to be a local minimum of the system until the limit of metastability for superheating $T = T^{**}$, the temperature at which $d^2f/d\phi^2 = 0$ at $\phi_{min} = 0$ and none of the AF1 phase can exist. It is these superheating and supercooling effects that give rise to the hysteresis in experimental observables with respect to the control parameters.

The hysteretic evolution of the oscillator strength with temperature for both pure and zinc alloyed samples can be explained with reference to the free energy diagram in Fig. 5, and the nomenclature used to describe hysteresis of disorder-broadened first-order phase transitions outlined in reference [38]. In the case of an ideally pure compound and in the absence of temperature fluctuations, the high or low temperature states can be taken to the limit of metastability at T^* and T^{**} respectively, where the phase transition occurs as a sharp discontinuity in the hysteretic parameter being observed.

In any real system, temperature fluctuations will perturb the system and destroy the metastable state at some intermediate temperature between T_N and T^* or T^{**}. The small amount of disorder present in any real crystal from impurities or defects will also cause a slight rounding of the transition. Both of these effects are observable in the hysteresis of pure CuO in Fig. 4(a). On heating, the electromagnon excitation emerges at temperature T_1, signifying the onset of nucleation of the AF2 phase, and grows in strength until reaching a maximum at 213.4 K. On cooling, the electromagnon strength begins to differ from that observed during heating around 213.4 K, signifying this temperature as T^{**}, and begins to decrease in strength

at temperature T_3 signifying the onset of nucleation of the AF1 phase. The temperature at which the electromagnon strength reduces to zero on cooling can therefore be identified as T^*. The system is observed to be in the metastable state for superheating and supercooling over a temperature range of $0.4\,\mathrm{K}$ in both cases. Similar trends can be seen for the zinc alloyed sample in Fig. 4(b), however in this case the phase transition is broadened by spin-disorder. The metastable phases for superheating and supercooling are also broadened upon zinc alloying, with both increasing to a width of $1\,\mathrm{K}$.

As discussed previously, simulations of the magnetic interactions in alloyed CuO showed a decrease in the energy difference between the AF1 and AF2 states relative to pure CuO [35]. However, the metastable phase observed in the zinc alloyed sample is wider than the pure sample. This may be partially due to smaller thermal fluctuations at the lower Néel temperatures of the alloyed sample, but could also be due to modifications to the exchange coupling parameters on alloying altering the form of the free energy barrier between the two phases. Modification of the biquadratic exchange and higher order coupling terms by the non-magnetic ions, as discussed in terms of the "order-by-disorder" mechanism above, could therefore possibly alter the free energy barrier height and increase the stability of the metastable phases in the zinc alloyed sample.

Conclusion

Here we reported for the first time that the dynamic magnetoelectric response at terahertz frequencies can be used to probe hysteresis and spin-disorder broadening at magnetic phase transitions. The oscillator strength $\Delta\epsilon$ of the electromagnon in $Cu_{1-x}Zn_xO$ was taken to represent the fraction of the magnetically-induced ferroelectric phase, AF2. By precisely tracking $\Delta\epsilon$ on cooling or heating across the phase transition between the commensurate AF1 phase and the ferroelectric AF2 phase we observed thermal hysteresis, indicating the first-order nature of this transition. The limits of metastability for superheating and supercooling were identified, and the metastable region was found to broaden for the alloy with greater spin-disorder. Alloying also enhanced the electromagnon energy from $3.0\,\mathrm{meV}$ to $3.7\,\mathrm{meV}$, potentially as a result of enhanced DM interaction or greater single-ion anisotropy. The results were discussed within the context of a simple Landau theory of a first-order phase transition, with reference to recent advances in phenomenological and first-principles theoretical models of CuO.

This work may have immediate impact by providing a new way to study the nature of magnetic phase transitions in multiferroics. In the longer term the increased understanding of multiferroics yielded by ultrafast spectroscopic methods, including terahertz time-domain spectroscopy, may help develop new magnetoelectric and multiferroic materials for spintronic applications.

References

[1] M. P. Kostylev, A. A. Serga, T. Schneider, B. Leven, and B. Hillebrands. Spin-wave logical gates. *Applied Physics Letters*, 87(15):153501, oct 2005.

[2] W. Tong, Y. Fang, J. Cai, S. Gong, and C. Duan. Theoretical studies of all-electric spintronics utilizing multiferroic and magnetoelectric materials. *Computational Materials Science*, 112:467–477, feb 2016.

[3] Zeila Zanolli. Graphene-multiferroic interfaces for spintronics applications. *Scientific Reports*, 6(1):31346, nov 2016.

[4] Martin Gajek, Manuel Bibes, Stéphane Fusil, Karim Bouzehouane, Josep Fontcuberta, Agnès Barthélémy, and Albert Fert. Tunnel junctions with multiferroic barriers. *Nature Materials*, 6(4):296–302, apr 2007.

[5] S. Y. Yang, J. Seidel, S. J. Byrnes, P. Shafer, C.-H. Yang, M. D. Rossell, P. Yu, Y.-H. Chu, J. F. Scott, J. W. Ager, L. W. Martin, and R. Ramesh. Above-bandgap voltages from ferroelectric photovoltaic devices. *Nature Nanotechnology*, 5(2):143–147, feb 2010.

[6] Hosho Katsura, Naoto Nagaosa, and Alexander V. Balatsky. Spin Current and Magnetoelectric Effect in Noncollinear Magnets. *Physical Review Letters*, 95(5):057205, jul 2005.

[7] M. Kenzelmann, A. B. Harris, S. Jonas, C. Broholm, J. Schefer, S. B. Kim, C. L. Zhang, S.-W. Cheong, O. P. Vajk, and J. W. Lynn. Magnetic Inversion Symmetry Breaking and Ferroelectricity in TbMnO 3. *Physical Review Letters*, 95(8):087206, aug 2005.

[8] T. Kimura, T. Goto, H. Shintani, K. Ishizaka, T. Arima, and Y. Tokura. Magnetic control of ferroelectric polarization. *Nature*, 426(6962):55–58, nov 2003.

[9] K.F. Wang, J.-M. Liu, and Z.F. Ren. Multiferroicity: the coupling between magnetic and polarization orders. *Advances in Physics*, 58(4):321–448, jul 2009.

[10] A. Pimenov, T. Rudolf, F. Mayr, A. Loidl, A. A. Mukhin, and A. M. Balbashov. Coupling of phonons and electromagnons in GdMnO 3. *Physical Review B*, 74(10):100403, sep 2006.

[11] A. Pimenov, A. A. Mukhin, V. Yu. Ivanov, V. D. Travkin, A. M. Balbashov, and A. Loidl. Possible evidence for electromagnons in multiferroic manganites. *Nature Physics*, 2(2):97–100, feb 2006.

[12] A. B. Sushkov, R. Valdés Aguilar, S. Park, S-W. Cheong, and H. D. Drew. Electromagnons in Multiferroic YMn 2 O 5 and TbMn 2 O 5. *Physical Review Letters*, 98(2):027202, jan 2007.

[13] Hosho Katsura, Alexander V. Balatsky, and Naoto Nagaosa. Dynamical Magnetoelectric Coupling in Helical Magnets. *Physical Review Letters*, 98(2):027203, jan 2007.

[14] N. Kida, Y. Takahashi, J. S. Lee, R. Shimano, Y. Yamasaki, Y. Kaneko, S. Miyahara, N. Furukawa, T. Arima, and Y. Tokura. Terahertz time-domain spectroscopy of electromagnons in multiferroic perovskite manganites [Invited]. *Journal of the Optical Society of America B*, 26(9):A35, sep 2009.

[15] S P Jones, S M Gaw, K I Doig, D Prabhakaran,

E M Hetroy Wheeler, A T Boothroyd, and J Lloyd-Hughes. High-temperature electromagnons in the magnetically induced multiferroic cupric oxide driven by intersublattice exchange. *Nature Communications*, 5:3787, 2014.

[16] Rogerio de Sousa and Joel E. Moore. Optical coupling to spin waves in the cycloidal multiferroic Bi Fe O 3. *Physical Review B*, 77(1):012406, jan 2008.

[17] A B Sushkov, M Mostovoy, R Valdés Aguilar, S-W Cheong, and H D Drew. Electromagnons in multiferroic RMn ₂ O ₅ compounds and their microscopic origin. *Journal of Physics: Condensed Matter*, 20(43):434210, oct 2008.

[18] R. Valdés Aguilar, M. Mostovoy, A. B. Sushkov, C. L. Zhang, Y. J. Choi, S-W. Cheong, and H. D. Drew. Origin of Electromagnon Excitations in Multiferroic R MnO 3. *Physical Review Letters*, 102(4):047203, jan 2009.

[19] S. P. P. Jones, N. C. Wurz, M. Failla, D. Prabhakaran, C. F. McConville, and J. Lloyd-Hughes. Influence of nonmagnetic Zn substitution on the lattice and magnetoelectric dynamical properties of the multiferroic material CuO. *Physical Review B*, 90(6):064405, 2014.

[20] Filip Kadlec, Christelle Kadlec, Jakub Vít, Fedir Borodavka, Martin Kempa, Jan Prokleška, Josef Buršík, Róbert Uhrecký, Stéphane Rols, Yi Sheng Chai, Kun Zhai, Young Sun, Jan Drahokoupil, Veronica Goian, and Stanislav Kamba. Electromagnon in the Z -type hexaferrite (Ba x Sr 1 x) 3 Co 2 Fe 24 O 41. *Physical Review B*, 94(2):024419, jul 2016.

[21] T. Kimura, Y. Sekio, H. Nakamura, T. Siegrist, and A. P. Ramirez. Cupric oxide as an induced-multiferroic with high-TC. *Nature Materials*, 7(4):291–294, apr 2008.

[22] J B Forsyth, P J Brown, and B M Wanklyn. Magnetism in cupric oxide. *Journal of Physics C: Solid State Physics*, 21(15):2917–2929, may 1988.

[23] M Ain, A Menelle, B M Wanklyn, and E F Bertaut. Magnetic structure of CuO by neutron diffraction with polarization analysis. *Journal of Physics: Condensed Matter*, 4(23):5327–5337, jun 1992.

[24] R. Villarreal, G. Quirion, M. L. Plumer, M. Poirier, T. Usui, and T. Kimura. Magnetic Phase Diagram of CuO via High-Resolution Ultrasonic Velocity Measurements. *Physical Review Letters*, 109(16):167206, oct 2012.

[25] M. Ain, W. Reichardt, B. Hennion, G. Pepy, and B. M. Wanklyn. Magnetic excitations in CuO. *Physica C: Superconductivity*, 162-164:1279–1280, dec 1989.

[26] A. T. Boothroyd, A. Mukherjee, S. Fulton, T. G. Perring, R. S. Eccleston, H. A. Mook, and B. M. Wanklyn. High-energy magnetic excitations in CuO. *Physica B: Condensed Matter*, 234-236:731–733, jun 1997.

[27] T. Shimizu, T. Matsumoto, A. Goto, T. V. Chandrasekhar Rao, K. Yoshimura, and K. Kosuge. Spin susceptibility and superexchange interaction in the antiferromagnet CuO. *Physical Review B*, 68(22):224433, dec 2003.

[28] D. A. Yablonskii. Mean-field theory of magnetic order in cupric oxide. *Physica C: Superconductivity*, 171(5-6):454–456, nov 1990.

[29] A Junod, D Eckert, G Triscone, J Mller, and W Reichardt. A study of the magnetic transitions in CuO: specific heat (1-330 K), magnetic susceptibility and phonon density of states. *Journal of Physics: Condensed Matter*, 1(43):8021–8034, oct 1989.

[30] J. W Loram, K. A Mirza, C. P Joyce, and A. J Osborne. Specific-Heat Evidence for Quasi-1D Magnetic Order in CuO. *Europhysics Letters (EPL)*, 8(3):263–268, feb 1989.

[31] E Gmelin, U Köbler, W Brill, T Chattopadhyay, and S Sastry. Magnetic specific heat and susceptibility of cupric oxide (CuO) single crystals. *Bulletin of Materials Science*, 14(2):117–123, apr 1991.

[32] S. L. Johnson, R. A. de Souza, U. Staub, P. Beaud, E. Möhr-Vorobeva, G. Ingold, A. Caviezel, V. Scagnoli, W. F. Schlotter, J. J. Turner, O. Krupin, W.-S. Lee, Y.-D. Chuang, L. Patthey, R. G. Moore, D. Lu, M. Yi, P. S. Kirchmann, M. Trigo, P. Denes, D. Doering, Z. Hussain, Z.-X. Shen, D. Prabhakaran, and A. T. Boothroyd. Femtosecond Dynamics of the Collinear-to-Spiral Antiferromagnetic Phase Transition in CuO. *Physical Review Letters*, 108(3):037203, jan 2012.

[33] Gianluca Giovannetti, Sanjeev Kumar, Alessandro Stroppa, Jeroen van den Brink, Silvia Picozzi, and José Lorenzana. High- T c Ferroelectricity Emerging from Magnetic Degeneracy in Cupric Oxide. *Physical Review Letters*, 106(2):026401, jan 2011.

[34] Xavier Rocquefelte, Karlheinz Schwarz, Peter Blaha, Sanjeev Kumar, and Jeroen van den Brink. Room-temperature spin-spiral multiferroicity in high-pressure cupric oxide. *Nature Communications*, 4:ncomms3511, sep 2013.

[35] J. Hellsvik, M. Balestieri, T. Usui, A. Stroppa, A. Bergman, L. Bergqvist, D. Prabhakaran, O. Eriksson, S. Picozzi, T. Kimura, and J. Lorenzana. Tuning order-by-disorder multiferroicity in CuO by doping. *Physical Review B*, 90(1):014437, jul 2014.

[36] Daniel Hone, P. A. Montano, T. Tonegawa, and Y. Imry. Three-dimensional ordering of impure linear-chain systems. *Physical Review B*, 12(11):5141–5149, dec 1975.

[37] Sindhunil Barman Roy. First order magneto-structural phase transition and associated multi-functional properties in magnetic solids. *Journal of Physics: Condensed Matter*, 25(18):183201, may 2013.

[38] S. B. Roy and P. Chaddah. Phase-coexistence and glass-like behavior in magnetic and dielectric solids with long-range order. *physica status solidi (b)*, 251(10):2010–2018, oct 2014.

[39] Yoseph Imry and Michael Wortis. Influence of quenched impurities on first-order phase transitions. *Physical Review B*, 19(7):3580–3585, apr 1979.

[40] Alex Soibel, Eli Zeldov, Michael Rappaport, Yuri Myasoedov, Tsuyoshi Tamegai, Shuuichi Ooi, Marcin Konczykowski, and Vadim B. Geshkenbein. Imaging the vortex-lattice melting process in the presence of disorder. *Nature*, 406(6793):282–287, jul 2000.

[41] Kun Cao, Feliciano Giustino, and Paolo G. Radaelli. Theory of Electromagnons in CuO. *Physical Review Letters*, 114(19):197201, may 2015.

[42] D. Prabhakaran and A. T. Boothroyd. Single crystal growth of Zn-doped CuO by the floating-zone method. *Journal of Crystal Growth*, 250(1-2):77–82, mar 2003.

[43] P.U. Jepsen, D.G. Cooke, and M. Koch. Terahertz spectroscopy and imaging - Modern techniques and applications. *Laser & Photonics Reviews*, 5(1):124–166, 2011.

[44] James Lloyd-Hughes and Tae-In Jeon. A Review of the Terahertz Conductivity of Bulk and Nano-Materials. *Journal of Infrared, Millimeter, and Terahertz Waves*, 33(9):871–925, sep 2012.

[45] C. D. W. Mosley, M. Failla, D. Prabhakaran, and J. Lloyd-Hughes. Terahertz spectroscopy of anisotropic materials using beams with rotatable polarization. *Scientific Reports*, 7(1):12337, dec 2017.

[46] Martin van Exter, Ch. Fattinger, and D. Grischkowsky. Terahertz time-domain spectroscopy of water vapor. *Optics Letters*, 14(20):1128, oct 1989.

[47] Christopher L. Henley. Ordering due to disorder in a frustrated vector antiferromagnet. *Physical Review Letters*, 62(17):2056–2059, apr 1989.

[48] A. B. Harris. Landau analysis of the symmetry of the magnetic structure and magnetoelectric interaction in

multiferroics. *Physical Review B*, 76(5):054447, aug 2007.

[49] M. L. Plumer. Nonlocal Landau theory of the magnetic phase diagram of highly frustrated magnetoelectric CuFeO 2. *Physical Review B*, 78(9):094402, sep 2008.

[50] G. Quirion and M. L. Plumer. Landau theory of the magnetic phase diagram of monoclinic multiferroics: Application to MnWO 4 and CuO. *Physical Review B*, 87(17):174428, may 2013.

Acknowledgements